Electronic Supplementary Information

Impact of Growth Phases on Photochemically Produced Reactive Species in the Extracellular Matrix of Algal Cultivation Systems

Raul Tenorio,[a,b] Anna C. Fedders,[a] Timothy J. Strathmann,[b] Jeremy S. Guest,[a,*]

[a.] Department of Civil and Environmental Engineering, University of Illinois at Urbana-Champaign, 205 North Mathews Avenue, 3221 Newmark Civil Engineering Laboratory, Urbana, Illinois 61801, USA

[b.] Department of Civil and Environmental Engineering, Colorado School of Mines, 1012 14th Street, Coolbaugh Hall, Golden, Colorado 80401, USA

*Corresponding author: Email: jsguest@illinois.edu, Phone: (217) 244-9247

26 pages, 10 tables, and 11 figures

Contents

S1. Materials and Methods

S1.1 Chemical Reagents. Benzene (BZ), 2,4,6-trimethylphenol (TMP), and furfuryl alcohol (FFA) were obtained from Sigma-Aldrich and used as molecular probes for quantifying reactive species. All pH adjustments were made using HCl (Macron Fine Chemicals) and NaOH (Sigma Aldrich). Total carbonate ($C_{T,CO3}$) was added using $NaHCO_3$ (Fisher Scientific). Suwannee river natural organic matter (SRNOM; reverse osmosis isolate) was obtained from the International Humic Substances Society and used as a representative example of terrestrial organic matter. Methanol (Fisher Scientific), acetonitrile (Macron Fine Chemicals), orthophosphoric acid (Sigma-Aldrich), and acetic acid (Sigma-Aldrich) were used to prepare eluents for liquid chromatography analysis. Growth medium was prepared from NH_4Cl (Amresco), $MgSO_4 \cdot 7H_2O$ (Fluka), $CaCl_2 \cdot H_2O$ (Fluka), K_2HPO_4 (Sigma-Aldrich), KH_2PO_4 (Sigma-Aldrich), EDTA (Sigma-Aldrich); $(NH_4)6Mo_7O_{24} \cdot 4H2O$ (Acros Organics), Na_2SeO_3 (Sigma-Aldrich), $ZnSO_4 \cdot 7H_2O$ (Sigma-Aldrich), $MnCl_2 \cdot 4H_2O$ (Sigma-Aldrich), Na_2CO_3 (Sigma-Aldrich), $FeCl_3 \cdot 6H_2O$ (Sigma-Aldrich), $CuCl_2 \cdot 2H_2O$ (Sigma-Aldrich), and $NaHCO_3$ (Fisher Scientific). All solutions were made using deionized water (Nanopure system; resistivity >18 MΩ-cm).

S1.2 Photobioreactor Schematic and Photo.

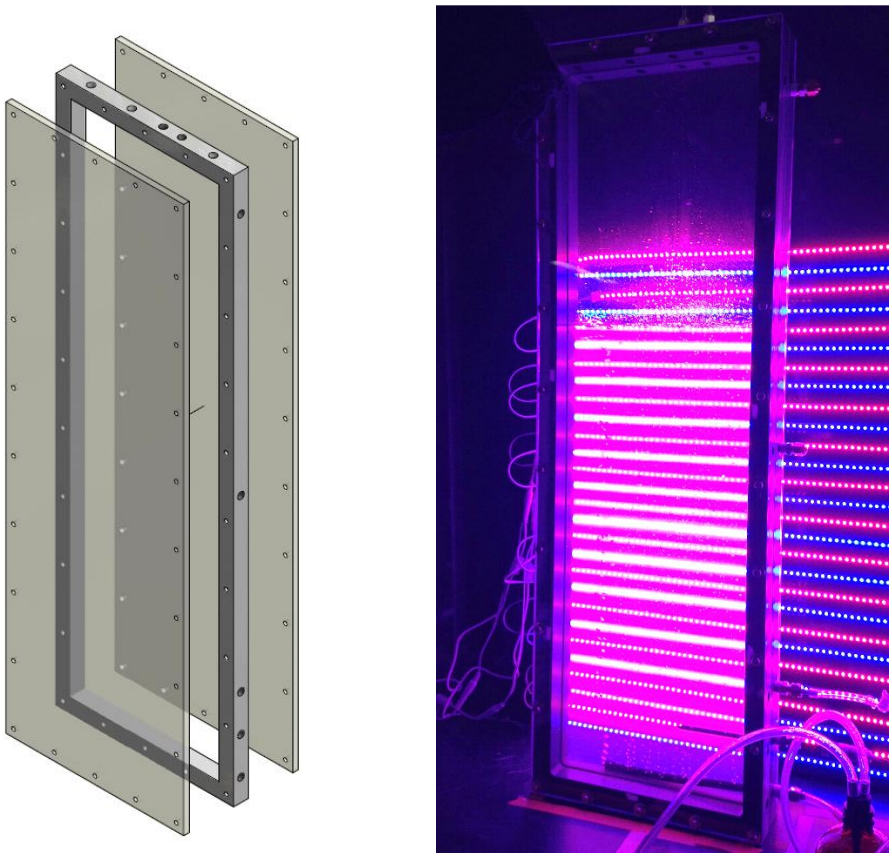

Figure S1. Photobioreactor schematic (left) and photo (right). Figure (left) provided by Jennifer Debellis.

S1.3 N-Protein Factor Calculation. The N-protein factor is the ratio of amino acid residues to the total nitrogen in the biomass,[1]

$$N\text{-}protein\ factor = M_R/M_N \tag{1}$$

where M_R is the total mass of amino acid residues and M_N is the total mass of nitrogen. M_R was calculated using the following equation

$$M_R = \sum_i x_{R,i} \cdot Mw_i \tag{2}$$

where $x_{R,i}$ is the amino acid mole fraction in *Chlamydomonas reinhardtii* under autotrophic conditions[2] and Mw_i is the molecular weight of the amino acid residue. The index refers to each amino acid in the biomass composition. Residue molecular weight was determined by subtracting the molecular weight of water (18 $g \cdot mol^{-1}$) from the molecular weight of the amino acid. M_N was calculated using the following equation,

$$M_N = \sum_i x_{R,i} \cdot M_{N,i} \tag{3}$$

where $M_{N,i}$ is the molecular weight of nitrogen (14 $g \cdot mol^{-1}$) multiplied by number of nitrogen atoms in the amino acid residue. N-protein factors were used to obtain protein concentrations ($g \cdot L^{-1}$) in *C. reinhardtii* biomass samples as follows

$$Protein\ (g \cdot L^{-1}) = N\text{-}protein\ factor \cdot f_N \cdot VSS\ (g \cdot L^{-1}) \tag{4}$$

where f_N is the mass fraction of nitrogen measured from CHN analysis, and VSS is the measured volatile suspended solids.

S1.4 Chemical Probe Measurement - HPLC Details. TMP, phenol, and FFA were measured by high performance liquid chromatography (HPLC) equipped with a photodiode array detector (SPD-M10Avp, Shimadzu). Separation was achieved using a Spherisorb 5 μm ODS2 4.6 × 150 mm column with a 4.6 × 10 mm guard cartridge of the same material. Phenol was analyzed at λ = 270 nm using a 35/65 mixture of acetonitrile and ~0.17 mM acetic acid aqueous solution (pH = 5, adjusted with NaOH). TMP was analyzed at λ = 277 nm using a 60/40 mixture of methanol and 10 mM orthophosphoric acid aqueous solution (pH = 2). FFA was analyzed at λ = 214 nm with a 20/80 mixture of acetonitrile and ~0.17 mM acetic acid aqueous solution (pH = 5, adjusted with NaOH). All HPLC methods used isocratic flow (1.0 $mL \cdot min^{-1}$).

S1.5 Light-Screening Correction Factor. TMP pseudo first-order rate constants ($k_{obs,TMP}$), hydroxyl radical formation rates ($R^{HO\bullet}$), and steady-state singlet oxygen concentrations ($[^1O_2]_{ss}$) were corrected for light-screening effects. Here we provide the derivation for light screening correction factors as described by Grandbois et al.[3]

Increasing dissolved organic matter (DOM) concentrations reduces quantified reactive species (RS) levels due to organic matter light screening, so RS must be corrected. The screening factor is a comparison of light intensity at the surface of a solution with the average light intensity throughout the full depth of the solution. The rate of light absorption for a thin solution (i.e., no light screening) ($k_{obs,thin}$) is defined as

$$k_{obs,thin} = 2.303 \sum_{\lambda} a_\lambda I_\lambda \tag{5}$$

where λ is the wavelength, a_λ is the absorption coefficient at given wavelength (cm^{-1}), and I_λ is the surface photon irradiance at a given wavelength ($E \cdot m^{-2} \cdot s^{-1}$). The rate of light absorption for a solution ($k_{obs,thick}$) with thickness z (cm) is defined as

$$k_{obs,thick} = 2.303 \sum_{\lambda} a_\lambda \langle I_\lambda \rangle_z \tag{6}$$

Where $\langle I_\lambda \rangle_z$ is the average photon irradiance over a thick solution with thickness z. $\langle I_\lambda \rangle_z$ is calculated by multiplying the surface photon irradiance I_λ by the light screening factor S_λ.

$$S_\lambda = \frac{1 - 10^{-a_\lambda z}}{2.303 a_\lambda z} \tag{7}$$

$$\langle I_\lambda \rangle_z = I_\lambda S_\lambda = I_\lambda \frac{1 - 10^{-a_\lambda z}}{2.303 a_\lambda z} \tag{8}$$

The value of a_λ was obtained using a spectrophotometer[4] and z was obtained by measuring the solution thickness in glass tubes for benzene experiments (z_{tube} = 1.0 cm) and calculated for beakers (z_{beaker} = 3.0 cm) for TMP and FFA experiments (Section S1.9). To obtain light screening correction factors (CF), we divide $k_{obs,thin}$ by $k_{obs,thick}$.

$$CF = \frac{k_{obs,thin}}{k_{obs,thick}} = \frac{\sum_\lambda a_\lambda I_\lambda}{\sum_\lambda a_\lambda \langle I_\lambda \rangle_z} \tag{9}$$

Corrected RS values (i.e., $k_{obs,TMP}$, $R^{HO\bullet}$, and $[^1O_2]_{ss}$) are obtained simply by multiplying measured values by CF. Table S1 shows an example calculation for obtaining light-screening CFs as shown in Romero et al. where the derivation by Grandbois et al. was also used.[3,5]

Table S1. Light-screening correction factor sample calculations for an EOM solution collected at day 10 (July 2015 replicate).

z_{tube} (cm)	1.0
z_{beaker} (cm)	3.0

$k_{obs,thin}$	$k_{obs,thick}$	
2.15E-05	1.73E-05	1.22E-05

Wavelength (nm)	Photon Irradiance (I_λ) ($E \cdot m^{-2} \cdot s^{-1}$)	Abs. (a_λ) EOM Day 10	S_λ Tube	S_λ Beaker	$a_\lambda \cdot I_\lambda$	$a_\lambda \cdot I_\lambda \cdot S_\lambda$ Tube	$a_\lambda \cdot I_\lambda \cdot S_\lambda$ Beaker
310	7.30E-08	0.419	0.631	0.326	3.06E-08	1.93E-08	9.98E-09
311	7.74E-08	0.414	0.634	0.330	3.20E-08	2.03E-08	1.06E-08
312	7.16E-08	0.409	0.637	0.333	2.93E-08	1.86E-08	9.75E-09
313	8.10E-08	0.401	0.642	0.338	3.25E-08	2.09E-08	1.10E-08
314	8.17E-08	0.397	0.645	0.341	3.24E-08	2.09E-08	1.11E-08
315	8.49E-08	0.391	0.649	0.346	3.32E-08	2.15E-08	1.15E-08
316	1.04E-07	0.385	0.653	0.349	4.02E-08	2.62E-08	1.40E-08
317	1.08E-07	0.380	0.656	0.353	4.11E-08	2.70E-08	1.45E-08
318	1.22E-07	0.375	0.659	0.357	4.56E-08	3.01E-08	1.63E-08
319	1.26E-07	0.370	0.663	0.361	4.67E-08	3.09E-08	1.68E-08

Irradiance was obtained using spectroradiometer and applying a 280 nm longpass filter. Absorbance was obtained using a spectrophotometer. Actual spreadsheet contains calculations from λ = 310-400 nm.

Table S2. Summary of light-screening correction factors in EOM and SRNOM solutions. EOM correction factors represent the average of values from January 2015 and July 2015 replicates.

EOM

Day	Correction Factor	
	Tube	Beaker
0	1.02	1.06
1	1.02	1.06
2	1.04	1.11
3	1.05	1.16
4	1.07	1.22
6	1.13	1.38
8	1.18	1.55
10	1.25	1.77

SRNOM Equivalent

Day	Correction Factor	
	Tube	Beaker
0	1.03	1.10
---	---	---
2	1.12	1.36
---	---	---
4	1.25	1.79
6	1.49	2.60
---	---	---
10	2.52	6.24

S1.6 Dark Controls. Dark controls for all chemical probes were performed in EOM and SRNOM solutions to detect non-photolytic probe decay using the same solution conditions as described above (data presented in Figure S2). As a conservative measure, dark controls were performed at the highest DOC_{EOM} observed (106 mg-C·L^{-1}; 95.2 mg-C·L^{-1} after diluting to 90%, $v_{sample} \cdot v_{final}^{-1}$, in irradiation experiments). Solutions were stored in 2 mL vials covered with foil at room temperature overnight before analysis.

Dark TMP decay pathways in EOM and SRNOM solutions were not observed; variation in TMP concentration was within one standard deviation of triplicate pre-irradiation samples in photolysis experiments. Small quantities of phenol were detected in EOM and SRNOM solution dark controls and were also detected in pre-irradiation samples in photolysis experiments; thus, only phenol production under irradiation was used in $R^{HO\bullet}$ calculations (i.e., $[phenol]_{t=0}$ - $[phenol]_t$). Dark FFA decay pathways were not observed in the SRNOM solution. However, 20% FFA decay (compared to the deionized water control) was observed in the EOM solution after 33 h in the dark. But because ~57% decay of FFA was observed after 4 h of irradiation (with light screening correction factors applied), FFA still decays significantly through photoproduced $^1O_2$ pathways.

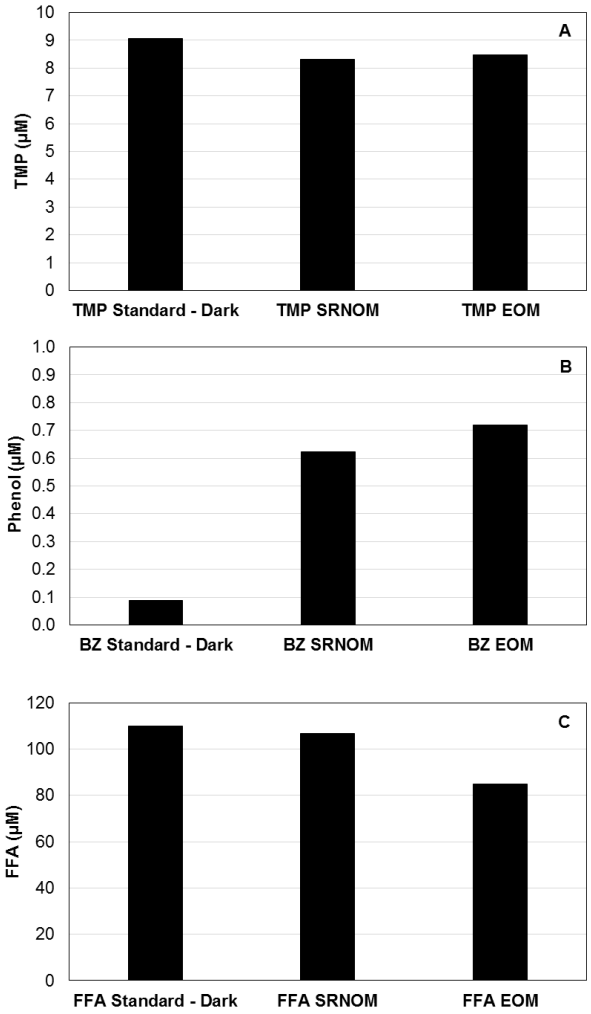

Figure S2. Dark controls for (A) TMP, (B) BZ, and (C) FFA. Standards (left columns) represent data from experiments in which the probe was added to deionized water at initial concentrations ($[TMP]_0$ = 10 µM, $[BZ]_0$ = 1 mM, $[FFA]_0$ = 100 µM). SRNOM solutions (middle columns) included Fe^{3+}, EDTA, and $NaHCO_3$ at concentrations similar to those measured in EOM solutions collected at day 10. EOM solutions (right columns) were collected at day 10 (July 2015 replicate). 2 mL vials of all solutions were covered with foil at room temperature overnight and analyzed after 11 h (TMP), 15 h (BZ), and 33 h (FFA). Analysis times vary due to instrument availability.

S1.7 Photosensitized Reactive Species Quantification. Reactive species generation was measured under simulated solar irradiation in an Atlas Suntest XLS+ solar simulator equipped with a xenon lamp filtered through a 310 nm longpass cutoff filter (Atlas, 56052372). Solutions were irradiated in 50 mL glass beakers wrapped in black tape to limit unintended light reflection.[5] A 280 nm longpass cutoff filter (Newport, FSQ-WG280) was placed over top of each beaker to limit evaporation and allow penetration of the full solar spectrum. Solutions were continuously mixed (300 rpm) on a 12-point stir plate (Variomag). All reactors were spaced evenly in a temperature-controlled water bath inside of the solar simulator to maintain temperature at 25 °C. Incident irradiance on the individual reactors was 398 ± 11 $W \cdot m^{-2}$

(integrated over 250-750 nm) as measured by spectroradiometer. Reactions for HO• production were performed in capped borosilicate tubes (16 × 150 mm) to limit volatilization of the benzene molecular probe scavenger.[6] Spectroradiometer measurements, reactor positions in the solar simulator, and the irradiance spectrum are discussed in detail in Section S1.8.

S1.8 Solar Simulator Characterization. Solar simulator irradiance was characterized by measuring light intensity using a spectroradiometer (Spectrilight ILT950, International Light Technologies) in 12 positions inside the solar simulator chamber. The spectroradiometer sensor was placed at each position and light intensity was measured in triplicate. The chamber area was divided into 12 evenly spaced positions to spatially characterize lamp irradiation. The positions correspond to reactor spacing and are displayed in Table S3.

Table S3. Top-down view of 12 reactor positions and average irradiance (in parentheses, $W \cdot m^{-2}$) in the solar simulator chamber. The numbered (bold) boxes represent evenly-spaced positions in the chamber where reactors were placed. Shaded boxes indicate positions used for TMP and FFA experiments.

1 (309)	**2** (308)	**3** (287)	**4** (282)
5 (383)	**6** (390)	**7** (390)	**8** (373)
9 (395)	**10** (413)	**11** (411)	**12** (391)

Front of Chamber

The six locations with the highest average irradiation were chosen to provide maximum light intensity for three TMP triplicates (positions 6, 9, 10) and three FFA triplicates (positions 7, 11, 12) experiments conducted simultaneously. The average irradiance of the six locations was 398 ± 11 $W \cdot m^{-2}$ (integrated over 250-750 nm) and the average irradiance spectrum is presented in Figure S3. Three borosilicate glass tubes used for benzene triplicate experiments were laid flat in the chamber evenly spaced with the bottom of tubes facing the front of the chamber. The irradiance on the glass tubes was assumed to be exposed to the same irradiation as TMP and FFA experiments. The integrated intensity over the wavelength range 310-400 nm was 40 $W \cdot m^{-2}$.

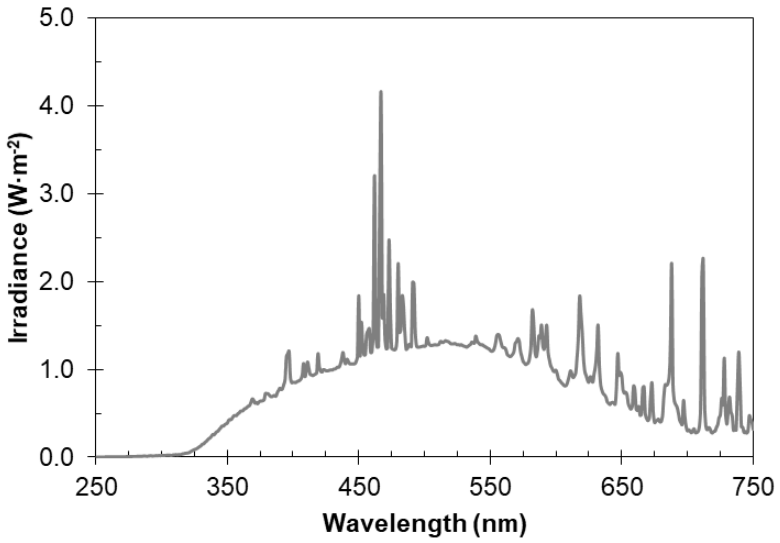

Figure S3. Irradiance spectrum obtained from spectroradiometer measurements. Measurements were made in triplicate at each reactor position and this spectrum represents the average across positions 6, 7, 9, 10, 11, and 12 (shaded boxes in Table S3).

S1.9 Calculating Average Pathlength. The average pathlength in BZ probe experiments for HO• quantification was assumed to be the diameter of the test tube (z = 1.0 cm). The average pathlength of TMP and FFA probe experiments (z_{avg}) performed in beakers for $^3DOM^*$ and $^1O_2$ quantification, respectively, was obtained by taking the mean of the longest possible pathlength based on the geometry of the beaker (z_l) and the solution depth, where the latter is assumed to be the shortest possible pathlength (z_d). The beaker geometry (Figure S4) and calculation used to obtain z_I and z_d are described below. The authors recognize that the effective pathlength in reactors – defined as the spatial average length of the light path taking into account reactor geometry and physics (i.e., light reflections, refraction, and scatter)[7,8] – may be slightly larger than the geometric pathlength. Beakers were wrapped in black tape, similar to other studies,[5,9–11] to minimize light reflections which would make the effective pathlength longer.

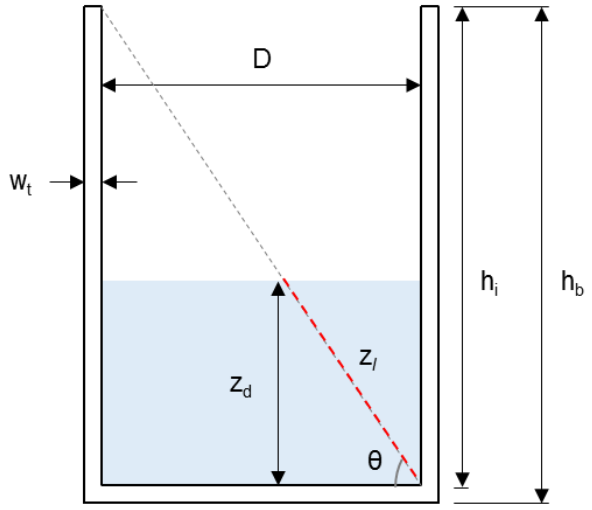

Figure S4. Beaker geometry used for estimated average pathlength, z_{avg}. D = diameter of the solution, w_t = beaker wall thickness throughout, h_i = inside-height of beaker, h_b = height of beaker, z_d = depth of solution, z_l = longest pathlength, θ = longest light path angle. The beaker measurements are as follows: w_t = 0.26 cm, h_b = 7.21 cm, z_d = 2.70 cm, V = 50 mL.

The inside-height of the beaker, h_i (6.95 cm), was calculated by,

$$h_i = h_b - w_t \tag{10}$$

the diameter of the water inside the beaker, D (4.86 cm), was calculated by,

$$D = 2\sqrt{\frac{V}{\pi\, z_d}} \tag{11}$$

the longest light path angle, θ (55.1°), was calculated by,

$$\theta = \tan^{-1}(h_i/D) \tag{12}$$

the longest pathlength, z_l (3.29 cm), was calculated by,

$$z_l = z_d/\sin\theta \tag{13}$$

and the average pathlength, z_{avg} (3.0 cm), was calculated using Equation 14.

$$z_{avg} = \frac{z_d + z_l}{2} \tag{14}$$

S2. Reactive Species Quantification: Determination of $[^1O_2]_{ss}$, $k_{obs,TMP}$, and $R^{HO\bullet}$

In this study, singlet oxygen ($^1O_2$), excited triplet state dissolved organic matter ($^3DOM^*$), and hydroxyl radicals (HO•) were quantified using steady-state concentrations of singlet oxygen ($[^1O_2]_{ss}$), pseudo first-order rate constants for 2,4,6-trimethylphenol (TMP) decay ($k_{obs,TMP}$), and hydroxyl radical production rates ($R^{HO\bullet}$), respectively. Here we describe quantification methods in detail for each reactive species (RS) using methods described elsewhere.[12]

RS are first photogenerated at a constant rate F. Then, the RS can pass through various reaction pathways: (1) unimolecular decay with first-order rate constant k_u, (2) bimolecular reaction with other compounds S_i in water with second-order rate constant k_{bi}, (3) bimolecular self-reaction with second-order rate constant k_{bs}, and (4) bimolecular reaction with probe P with second-order rate constant k_p. RS self-reaction is negligible in natural waters and can be ignored. The relationship between all reactions can be described using the following equations.

$$\frac{d[RS]}{dt} = F - [RS]\left(k_u + k_p[P] + \sum_i k_{bi}[S_i]\right) \tag{15}$$

$$\frac{d[P]}{dt} = -k_p[RS][P] \tag{16}$$

After applying steady-state approximation (d[RS]/dt = 0) and rearranging Equation 15, we obtain the following.

$$[RS]_{ss} = \frac{F}{k_u + k_p[P] + \sum_i k_{bi}[S_i]} \tag{17}$$

If probe concentrations are sufficiently low to leave $[RS]_{ss}$ unaffected ($k_p[P] \ll k_u + \Sigma_i k_{bi}[S_i]$), the rate of probe loss is then proportional to P.

$$\frac{d[P]}{dt} = -k_{obs}[P] \tag{18}$$

$$k_{obs} = k_p[RS]_{ss} \tag{19}$$

Integrating Equation 18, we obtain

$$ln\frac{[P]}{[P]_0} = -k_{obs}t \tag{20}$$

k_{obs} is obtained from the slope after plotting ln $[P]/[P]_0$ versus time. If k_p is known, then we can calculate $[RS]_{ss}$ using Equation 19.

S2.1 Singlet Oxygen ($^1O_2$). FFA reacts selectively with $^1O_2$ and the decay of FFA can be measured over time.[13,14] FFA decay is first-order with respect to $^1O_2$ and first-order with respect to FFA making the reaction second-order overall.[14]

$$\frac{-d[FFA]}{dt} = k_{^1O_2,FFA}[^1O_2][FFA] \tag{21}$$

$$k_{^1O_2,FFA} = 1.063 \times 10^8\ M^{-1} \cdot s^{-1} \tag{22}$$

Where $k_{1O2,FFA}$ is the second order-rate constant of $^1O_2$ and FFA published in Appiani et al. (1.00×10^8 $M^{-1}\cdot s^{-1}$ at 22 °C), adjusted to our experimental conditions (1.063×10^8 $M^{-1}\cdot s^{-1}$, 25 °C).[15]

Equation 21 follows pseudo first-order kinetics if [FFA] is sufficiently low to leave $[^1O_2]_{ss}$ constant. Under these conditions we obtain the following equations,

$$\frac{-d[FFA]}{dt} = k_{obs}[FFA] \tag{23}$$

$$k_{obs} = k_{^1O_2,FFA}[^1O_2]_{ss} \tag{24}$$

where k_{obs} is the observed pseudo first-order rate constant. Integrating Equation 23, we obtain

$$ln\frac{[FFA]}{[FFA]_o} = -k_{obs}t \tag{25}$$

k_{obs} is obtained from the slope after plotting ln $[FFA]/[FFA]_0$ versus time. Dividing k_{obs} by $k_{1O2,FFA}$ gives the steady-state singlet oxygen concentration ($[^1O_2]_{ss}$).

$$[^1O_2]_{ss} = \frac{k_{obs}}{k_{^1O_2,FFA}} \tag{26}$$

S2.2 Excited Triplet State Dissolved Organic Matter ($^3DOM^*$). TMP decays primarily via oxidation by $^3DOM^*$ by electron transfer[16] and pseudo first-order rate constants of TMP decay ($k_{obs,TMP}$) were measured as a surrogate for $^3DOM^*$ reactivity, similar to other recent studies.[10,11,17] After applying pseudo first-order kinetics (Equation 20), we obtain the following,

$$\frac{-d[TMP]}{dt} = k_{obs,TMP}[TMP] \tag{27}$$

where $k_{obs,TMP}$ is obtained from the slope after plotting ln $[TMP]/[TMP]_0$ versus time.

S2.3 Hydroxyl Radical (HO•). 4-chlorobenzoic acid (*p*CBA) is a molecular probe commonly used for $[HO•]_{ss}$ quantification.[18,19] Negligible *p*CBA decay occurred in irradiated extracellular organic matter (EOM) solutions preventing $[HO•]_{ss}$ quantification. Instead, the presence of HO• was investigated by quantifying hydroxyl radical production rates ($R^{HO•}$) using benzene (BZ) as a molecular probe. Benzene reacts with HO• to yield a stable phenol product that can be measured over time.[20] Benzene produced measurable concentrations of phenol throughout irradiation for all samples in this study allowing for comparison. Below is the procedure used to quantify the rate of HO• production ($R^{HO•}$). From phenol measurements, we can obtain a phenol production rate (d[phenol]/dt),

$$\frac{d[phenol]}{dt} = 0.85 \cdot k_{HO•,benzene}[HO\ •][benzene] \tag{28}$$

where $k_{HO•,benzene}$ is the second-order rate constant between benzene and HO• ($k_{HO•,benzene}$ = 7.8×10^9 $M^{-1}\cdot s^{-1}$) and 0.85 is the benzene to phenol conversion efficiency.[6,19,21] Applying the steady-state approximation to HO• formation rates leads to the following equation.

$$\frac{d[HO\ •]}{dt} = 0 = R^{HO•} - k_{HO•,benzene}[HO\ •][benzene] - \sum_i k_{HO•,S_i}[HO\ •][S_i] \tag{29}$$

S_i scavenges HO• with second-order rate constant, $k_{HO•,Si}$. After rearranging Equation 29, we obtain the following equation.

$$[HO\ •]_{ss} = \frac{R^{HO•}}{k_{HO•,benzene}[benzene] + \sum_i k_{HO•,S_i}[S_i]} \tag{30}$$

Substituting Equation 30 into Equation 28, we obtain the following.

$$\frac{d[phenol]}{dt} = 0.85 \cdot k_{HO•,benzene}[HO\ •][benzene] = \frac{0.85 \cdot k_{HO•,benzene}\ R^{HO•}\ [benzene]}{k_{HO•,benzene}[benzene] + \sum_i k_{HO•,S_i}[S_i]} \tag{31}$$

Utilizing a benzene concentration sufficiently high such that $k_{HO•,benzene}[benzene] \gg \Sigma_i\ k_{HO•,Si}[S_i]$, Equation 31 simplifies as follows.

$$R^{HO•} = \frac{1}{0.85} \cdot \frac{d[phenol]}{dt} \tag{32}$$

S2.4 HO• Scavenging. By rearranging Equation 31, we eliminate the assumption that $\Sigma\ k_{HO•,Si}\ [S_i] \ll k_{HO•,benzene}\ [benzene]$ and the equation becomes the following.

$$R_S^{HO•} = \frac{k_{HO•,\ benzene}[benzene] + \sum_i k_{HO•,S_i}[S_i]}{k_{HO•,\ benzene}[benzene]}\ \cdot R^{HO•} \tag{33}$$

where $R_s^{HO\bullet}$ is the hydroxyl radical production rate eliminating the assumption that $\Sigma k_{HO\bullet,Si}[S_i] \ll k_{HO\bullet,benzene}$ [benzene], $R^{HO\bullet}$ is the hydroxyl radical production rate assuming $\Sigma k_{HO\bullet,Si}[S_i] \ll k_{HO\bullet,benzene}$ [benzene] (Equation 32), and the numerator represents total HO• scavenging by all species where $\Sigma k_{HO\bullet,Si}[S_i]$ is the sum of HO• scavenging by species other than benzene, as follows.

$$\sum_i k_{HO\bullet,S_i}[S_i] = k_{HO\bullet,\ DOM}[DOM] + k_{HO\bullet,\ EDTA}[EDTA] + k_{HO\bullet,\ HCO_3^-}[HCO_3^-] + k_{HO\bullet,\ CO_3^{2-}}[CO_3^{2-}] \quad (34)$$

Because the second-order rate constant of HO• and EOM ($k_{HO\bullet,EOM}$) is not known, it was assumed to be similar to that of Pony lake fulvic acid (PLFA), an end-member reference material for autochthonous (microbial/algal derived) organic matter.[22,23] The limitations of this assumption are that EOM is a complex mixture and may have different HO• scavenging properties than PLFA because EOM is not an isolated subfraction (e.g., fulvic acid) of the original DOM, and EOM originates from algal cultivation (not an aquatic source as does PLFA). The $k_{HO\bullet,PLFA}$ found in other studies was $k_{HO\bullet,PLFA} = 3.29 \pm 1.87 \times 10^4$ L·(mg-C)$^{-1}$·s^{-1} (average and standard deviation)[23–26] and was used in this study as an estimate for $k_{HO\bullet,EOM}$. The average second-order rate constants of HO• and Suwannee river humic acid ($k_{HO\bullet,SRHA} = 1.90\times10^4$ L·(mg-C)$^{-1}$·s^{-1})[27] and fulvic acid ($k_{HO\bullet,SRFA} = 2.7\times10^4$ L·(mg-C)$^{-1}$·s^{-1})[27] was used as an estimate for the second-order rate constant of HO• and SRNOM ($k_{HO\bullet,SRNOM} = 2.3\times10^4$ L·(mg-C)$^{-1}$·s^{-1}). By using estimated $k_{HO\bullet,EOM}$ and $k_{HO\bullet,SRNOM}$ and also using the second-order rate constants of HO• and EDTA ($k_{HO\bullet,EDTA} = 2\times10^9$ M^{-1}·s^{-1}, pH = 9),[28] HO• and HCO_3^- ($k_{HO\bullet,HCO3-} = 8.5\times10^6$ M^{-1}·s^{-1}),[28] HO• and CO_3^{2-} ($k_{HO\bullet,CO32-} = 3.9\times10^8$ M^{-1}·s^{-1}),[28] and HO• and benzene ($k_{HO\bullet,benzene} = 7.8\times10^9$ M^{-1}·s^{-1}),[29] the percent contribution of HO• scavenging by each species can be calculated. The concentration and percent contribution to HO• scavenging of species in irradiated EOM and SRNOM solutions are presented in Table S4 and S5, respectively.

Table S4. HO• scavengers and concentrations in EOM solutions during irradiation and the contribution to scavenging (%) of each species. All concentrations represent those used during irradiation experiments (EOM samples diluted to 90%, $v_{sample} \cdot v_{final}^{-1}$).

DOC_{EOM} (mg-C·L^{-1})	DOC_{EDTA} (mg-C·L^{-1})	HCO_3^- (M)	CO_3^{2-} (M)	BZ (M)	% DOC_{EOM} Scavenging	% DOC_{EDTA} Scavenging	% HCO_3^- Scavenging	% CO_3^{2-} Scavenging	% BZ Scavenging
1.05	6.86	8.80E-03	3.68E-05	1.0E-03	0.4	1.4	0.9	0.2	97.0
1.68	6.86	7.71E-03	5.46E-05	1.0E-03	0.7	1.4	0.8	0.3	96.8
7.25	6.86	3.90E-03	3.79E-05	1.0E-03	2.9	1.4	0.4	0.2	95.1
12.64	6.86	3.83E-03	4.74E-05	1.0E-03	5.0	1.4	0.4	0.2	93.1
19.30	6.86	3.79E-03	5.08E-05	1.0E-03	7.4	1.3	0.4	0.2	90.7
38.38	6.86	3.79E-03	5.01E-05	1.0E-03	13.7	1.2	0.3	0.2	84.5
65.68	6.86	3.88E-03	5.07E-05	1.0E-03	21.3	1.1	0.3	0.2	77.0
97.48	6.86	3.88E-03	4.20E-05	1.0E-03	28.7	1.0	0.3	0.1	69.8

Table S5. HO• scavengers and concentrations in SRNOM solutions during irradiation and the contribution to scavenging (%) of each species. All concentrations represent those used during irradiation experiments; SRNOM solutions were adjusted to mimic DOC_{EOM}, Fe^{3+}, EDTA, and $NaHCO_3$ concentrations and pH in EOM solutions.

DOC_{SRNOM} (mg-C·L^{-1})	DOC_{EDTA} (mg-C·L^{-1})	HCO_3^- (M)	CO_3^{2-} (M)	BZ (M)	% DOC_{SRNOM} Scavenging	% DOC_{EDTA} Scavenging	% HCO_3^- Scavenging	% CO_3^{2-} Scavenging	% BZ Scavenging
1.90	6.86	3.91E-03	2.42E-05	1.00E-03	0.5	1.4	0.4	0.1	97.5
8.45	6.86	3.92E-03	4.85E-05	1.00E-03	2.4	1.4	0.4	0.2	95.6
19.10	6.86	3.90E-03	1.98E-05	1.00E-03	5.2	1.4	0.4	0.1	92.9
37.20	6.86	3.91E-03	2.35E-05	1.00E-03	9.7	1.3	0.4	0.1	88.5
100.35	6.86	3.92E-03	4.47E-05	1.00E-03	22.5	1.1	0.3	0.2	75.9

For all samples except where DOC_{EOM} = 38.4-97.5 mg-C·L^{-1} and DOC_{SRNOM} = 37.2-100 mg-C·L^{-1}, benzene scavenged greater than ~90% of HO•s. The numerator in Equation 33 predicts 69.8% HO• scavenging by benzene in the EOM solution at DOC_{EOM} = 97.5 mg-C·L^{-1} and 75.9% HO• scavenging by benzene in the SRNOM solution at DOC_{SRNOM} = 100 mg-C·L^{-1} where DOC_{EOM} and DOC_{SRNOM} contributed to 28.7% and 22.5% HO• scavenging in EOM and SRNOM solutions, respectively. Rearranging Equation 33, this corresponds to $R_s^{HO•}/R^{HO•}$ of 1.43 for the EOM solution and 1.32 for the SRNOM solution, meaning that the $R^{HO•}$ should be 43% and 32% greater for the EOM and SRNOM solutions, respectively, when accounting for EOM and SRNOM HO• scavenging rather than assuming $\Sigma\, k_{HO•,Si}\,[S_i] \ll k_{HO•,benzene}\,[benzene]$. Figure S5 shows the $R_s^{HO•}$ values compared to $R^{HO•}$ values presented in Figure 4 of the main text.

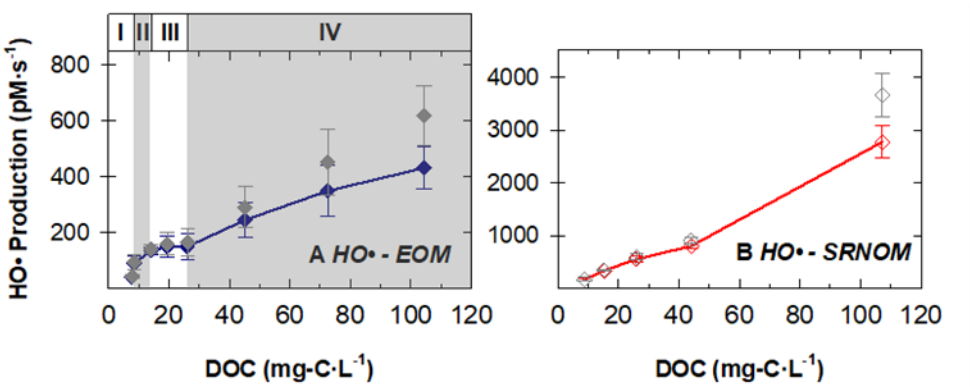

Figure S5. Effect of DOC (i.e., DOC_{EOM} + DOC_{EDTA} or DOC_{SRNOM} + DOC_{EDTA}) in (A) EOM and (B) SRNOM solutions on HO• production rates. Blue filled diamonds represent $R^{HO•}$ in EOM solutions and red hollow diamonds represent $R^{HO•}$ in SRNOM solutions, assuming $\Sigma\, k_{HO•,Si}\,[S_i] \ll k_{HO•,benzene}\,[benzene]$. All values were corrected for light screening. Grey filled diamonds represent $R_s^{HO•}$ in EOM solutions and grey hollow diamonds represent $R_s^{HO•}$ in SRNOM solutions, corrected for scavenging effects.

The benzene probe was added to test tubes at concentrations of 1 mM. Based on the rate constant assumptions, the benzene concentration required for at least 99% HO• scavenging by benzene would be 2.6-3.0 mM at the lowest DOC_{EOM} or DOC_{SRNOM} concentration (1.0-1.9 mg-C·L^{-1}) or 31-43 mM at the highest DOC_{EOM} or DOC_{SRNOM} concentration (97-100 mg-C·L^{-1}). The solubility of benzene is 1789 mg·L^{-1} (22.9 mM)[30] in water, thus, the latter concentration could not be achieved.

S2.5 FFA and TMP reaction with HO•. A kinetic calculation is presented here to estimate the contribution of HO• reaction to FFA decay ($^1O_2$ probe) and TMP decay ($^3DOM^*$ probe).

Because steady-state HO• concentrations ($[HO•]_{ss}$) were not measured directly, they were estimated using the following equation:

$$[HO\,•]_{ss} = \frac{R^{HO•}}{\sum_i k_{HO•,S_i}[S_i]} \tag{35}$$

where $R^{HO\bullet}$ is the hydroxyl radical production rate and $\Sigma k_{HO\bullet,Si}[S_i]$ is the sum of HO• scavenging species other than the benzene probe (Equation 34). The estimated $[HO\bullet]_{ss}$ using Equation 35 is 1.3-3.5×10^{-16} M if we assume benzene is in excess ($R^{HO\bullet}$; Equation 32) and 1.8-3.7×10^{-16} M if we do not assume benzene is in excess ($R_s^{HO\bullet}$; Equation 33). Thus, we can estimate $[HO\bullet]_{ss}$ is on the order of 10^{-16} M. With the estimated $[HO\bullet]_{ss}$, the following equation can be used to describe the contribution of HO• and $^1O_2$ to FFA decay:

$$k_{obs,FFA} = k_{HO\bullet,FFA}[HO\bullet] + k_{^1O_2,FFA}[^1O_2] \quad (36)$$

where $k_{obs,FFA}$ is the observed pseudo first-order rate constant of FFA decay (with light screening correction factors applied), $k_{HO\bullet,FFA}$ is the second-order rate constant of HO• and FFA ($k_{HO\bullet,FFA}$ = 1.5 × 10^{10} $M^{-1}\cdot s^{-1}$),[28] and $k_{1O2,FFA}$ is the second-order rate constant of $^1O_2$ and FFA. We can define percent of FFA decay by HO• reaction as follows:

$$\%\ FFA\ Decay = 100\left(\frac{k_{HO\bullet,FFA}[HO\bullet]}{k_{obs,FFA}}\right) \quad (37)$$

Similarly, the following equation can be used to describe the contribution of HO• and $^3DOM^*$ reaction to TMP decay:

$$k_{obs,TMP} = k_{HO\bullet,TMP}[HO\bullet] + k_{^3DOM^*,TMP}[^3DOM^*] \quad (38)$$

where $k_{obs,TMP}$ is the observed pseudo first-order rate constant of TMP decay (with light screening correction factors applied), $k_{HO\bullet,TMP}$ is the second-order rate constant of HO• and TMP, [HO•] is the steady-state concentration of HO•, $k_{3DOM^*,TMP}$ is the second-order rate constant of $^3DOM^*$ and TMP, and [$^3DOM^*$] is the steady-state concentration of $^3DOM^*$. We can assume the second-order rate constant of HO• and TMP is similar to that of phenols as described in another study (e.g., $k_{HO\bullet,phenol}$ = 1.8×10^{10} $M^{-1}\cdot s^{-1}$; $k_{HO\bullet,3\text{-methoxyphenol}}$ = 3.2x10^{10} $M^{-1}\cdot s^{-1}$).[16,28] The average of these two rate constants was used as an estimate for $k_{HO\bullet,TMP}$ (2.5×10^{10} $M^{-1}\cdot s^{-1}$). We can define percent of TMP decay by HO• reaction as follows.

$$\%\ TMP\ Decay = 100\left(\frac{k_{HO\bullet,TMP}[HO\bullet]}{k_{obs,TMP}}\right) \quad (39)$$

A summary of results for the estimated percent contribution of TMP and FFA decay by HO• reaction is shown in Table S6. For the growth phases of interest in this study (i.e., days 2-10) HO• plays a minimal role in TMP decay (3-7%) while HO• contributes up to 27% of FFA decay at day 2 but drops to 3% at day 10. Thus, there may be an overestimation of $^1O_2$ in the exponential growth phase. But TMP and FFA decay should be dominated by $^3DOM^*$ and $^1O_2$ reaction at days 4-10 (Fig. 3A and 3C) since the contribution by HO• was only 3-7% (TMP decay) and 3-16% (FFA decay) (Table S6).

Table S6. Percent of FFA ($^1O_2$ probe) decay and TMP ($^3DOM^*$ probe) decay contributed by HO• in EOM solutions. Estimated HO• concentrations were on the order of $[HO•]_{ss} = 10^{-16}$ M, thus this concentration was used in all calculations.

Day	DOC_{EOM} (mg-C·L^{-1})	DOC_{EDTA} (mg-C·L^{-1})	$[HO•]_{ss} \times k_{HO•,TMP}$ (s^{-1})	$k_{obs,TMP}$ (s^{-1})	$[HO•]_{ss} \times k_{HO•,FFA}$ (s^{-1})	$k_{obs,FFA}$ (s^{-1})	TMP % HO• reaction	FFA % HO• reaction
0	1.05	6.858	2.5E-06	1.12E-05	1.50E-06	5.81E-07	22.3	>100
1	1.68	6.858	2.5E-06	2.21E-05	1.50E-06	1.67E-06	11.3	89.8
2	7.25	6.858	2.5E-06	3.41E-05	1.50E-06	5.47E-06	7.3	27.4
3	12.6	6.858	2.5E-06	3.44E-05	1.50E-06	7.57E-06	7.3	19.8
4	19.3	6.858	2.5E-06	3.70E-05	1.50E-06	9.31E-06	6.8	16.1
6	38.4	6.858	2.5E-06	5.82E-05	1.50E-06	1.55E-05	4.3	9.7
8	65.7	6.858	2.5E-06	7.93E-05	1.50E-06	3.14E-05	3.2	4.8
10	97.5	6.858	2.5E-06	8.02E-05	1.50E-06	6.12E-05	3.1	2.5

S3. Photoreactivity Quantification: Determination of f_{TMP}, Φ_{1O2}, and $\Phi_{HO•}$

S3.1 $^3DOM^*$ Quantum Yield Coefficients (f_{TMP}). Values of f_{TMP} were calculated using the steps described in other studies.[16,31] If steady-state concentrations of $^3DOM^*$ ($[^3DOM^*]_{ss}$) are assumed, the rate of TMP and $^3DOM^*$ reaction (R_{TMP}) is as follows.

$$R_{TMP} = k_{3DOM*,TMP}[^3DOM^*]_{ss}[TMP] = k_{obs,TMP}[TMP] \quad (40)$$

Where $k_{3DOM*,TMP}$ is the second-order rate constant between $^3DOM^*$ and TMP and $k_{obs,TMP}$ is the observed pseudo first-order rate constant for TMP degradation (Equation 27). In this case, $[^3DOM^*]_{ss}$ is unknown, but the following relationship is known

$$[^3DOM^*]_{ss} = \frac{R_a \Phi_{3DOM*}}{\sum k_d} \quad (41)$$

where the numerator is the rate of $^3DOM^*$ formation (i.e., $R_p = R_a \Phi_{3DOM*}$), R_a is the rate of light absorption, Φ_{3DOM*} is the $^3DOM^*$ quantum yield, and Σk_d is the sum of all $^3DOM^*$-loss reaction rate constants. R_a is defined as follows,[32]

$$R_a = \sum_{\lambda} (E^0_{p,\lambda}(1 - 10^{-a_\lambda z})/z) \quad (42)$$

where $E^0_{p,\lambda}$ is the photon irradiance on the sample surface (mE·cm^{-2}·s^{-1}), a_λ is the organic matter absorption coefficient (cm^{-1}), and z is the pathlength (cm). The summation in Equation 42 was carried out for λ = 310-400 nm. $E^0_{p,\lambda}$ was determined using a spectroradiometer. a_λ were obtained from organic matter UV-vis absorbance measurements. The pathlength was z = 3.0 cm for $^3DOM^*$ experiments performed in beakers. By substituting Equation 41 into Equation 40 and rearranging, we obtain the following equation.

$$k_{obs,TMP} = \frac{k_{3DOM*,TMP} R_a \Phi_{3DOM*}}{\sum k_d} \quad (43)$$

Note that the $^3DOM^*$ formation rate ($R_p = R_a \Phi_{3DOM*}$) is embedded in the $k_{obs,TMP}$. If $k_{3DOM*,TMP}$, and Σk_d are assumed to be approximately constant for organic matter used in this study, f_{TMP} is written as follows.

$$f_{TMP} = k_{obs,TMP}/R_a = \frac{k_{3DOM*,TMP} \Phi_{3DOM*}}{\sum k_d} \quad (44)$$

$k_{obs,TMP}$ in Equation 44 was not corrected for light screening.

S3.2 $^1O_2$ Quantum Yields (Φ_{1O2}). Φ_{1O2} were calculated using a method described elsewhere.[32] The method uses the following equations.

$$\Phi_{1O2} = R_p/R_a \quad (45)$$

$$R_p = [^1O_2]_{ss} \cdot k_{d,H2O} \quad (46)$$

Where R_p is the rate of $^1O_2$ production, R_a is the rate of light absorption (Equation 42) obtained using a pathlength of z = 3.0 cm for $^1O_2$ experiments performed in beakers, and $k_{d,H2O} = 2.5\times10^5$ s^{-1} is the deactivation of $^1O_2$ by water.**[14]** $[^1O_2]_{ss}$ were obtained from previous calculations (Equation 26) and were not corrected for light screening in Equation 46.

S3.3 HO• Quantum Yields ($\Phi_{HO•}$). $\Phi_{HO•}$ were determined using a method described elsewhere.[6] However, it should be noted that Dong and Rosario-Ortiz used the specific rate of light absorption (in $E\cdot s^{-1}\cdot cm^{-3}\cdot M^{-1}$) which incorporates the apparent molar absorptivity of the excited compound and requires the specific rate of light absorption be multiplied by the excited compound concentration (in M) to obtain the units $Einstein\cdot s^{-1}\cdot cm^{-3}$, whereas this study used R_a from Equation 42 (Section S3.1, ESI) with units $mE\cdot cm^{-3}\cdot s^{-1}$ (i.e., $E\cdot L^{-1}\cdot s^{-1}$). The following equations were used to calculate $\Phi_{HO•}$.

$$\Phi_{HO•} = R_p/R_a \quad (47)$$

$$R_p = R^{HO•} \quad (48)$$

Where R_p is the rate of HO• production ($R^{HO•}$, not corrected for light screening) (Equation 32), and R_a is the rate of light absorption (Equation 42) obtained using a pathlength of z = 1.0 cm for HO• experiments performed in tubes.

S4. Additional Data

S4.1 Additional Algal Culture and Extracellular Organic Matter (EOM) Characterization.

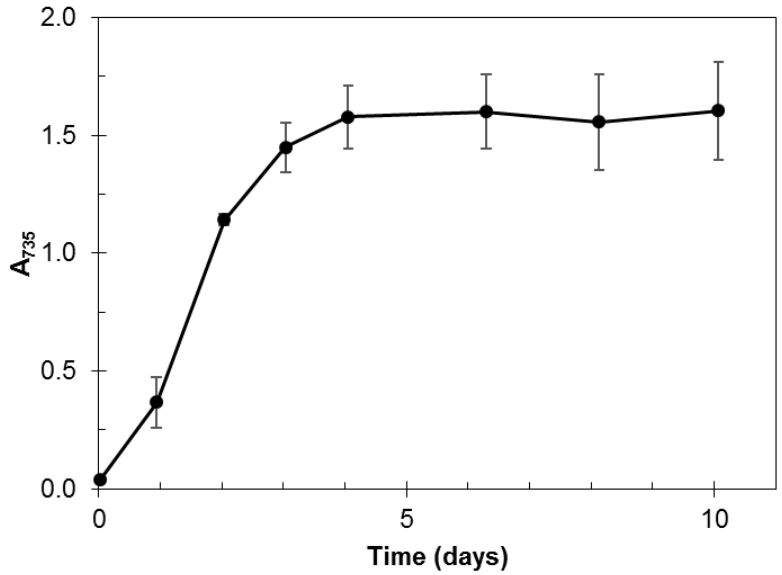

Figure S6. Cell growth throughout 10-day growth period represented as optical density (A_{735}; absorbance at 735 nm). Points represent the average of replicate cultivations (January 2015 and July 2015). Error bars extend to minimum and maximum measured values.

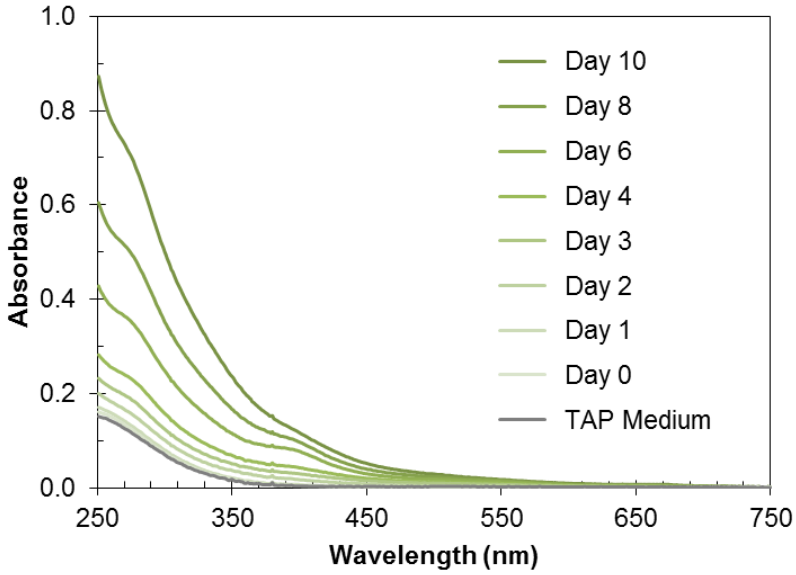

Figure S7. Average absorbance spectra for EOM solutions collected from January 2015 and July 2015 cultures. Spectra includes the absorbance of EOM and the absorbance of the background TAP growth medium at concentrations present in irradiation experiments (90% diluted, $v_{sample} \cdot v_{final}^{-1}$). The absorbance of TAP growth medium (90% diluted, $v_{sample} \cdot v_{final}^{-1}$) is shown for comparison.

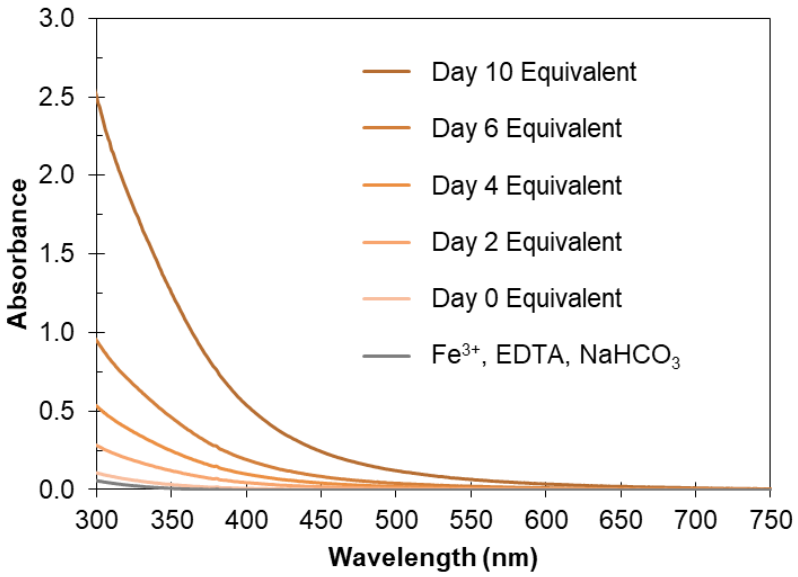

Figure S8. Absorbance spectra for Suwannee river natural organic matter (SRNOM) solutions adjusted to mimic DOC_{EOM}, Fe^{3+}, EDTA, and $NaHCO_3$ concentrations and pH in EOM solutions (DOC concentrations are listed in Table S8). The absorbance of a solution of Fe^{3+}, EDTA, and $NaHCO_3$ at concentrations and pH present in SRNOM solutions is shown for comparison.

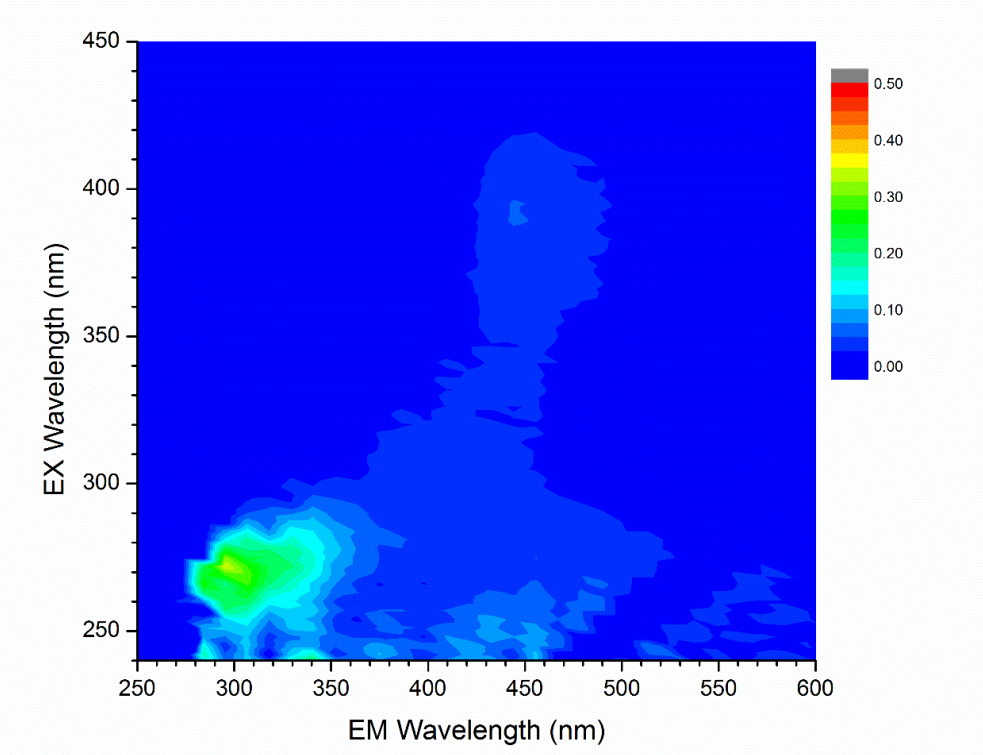

Figure S9. Excitation Emission Matrix (EEM) generated for 1 mg-C·L^{-1} (DOC_{EOM}; where DOC_{TOTAL} = DOC_{EOM} + DOC_{EDTA}) of EOM at day 0. EEMs spectra are in Raman units. EEM was generated for the EOM solution collected from the July 2015 culture.

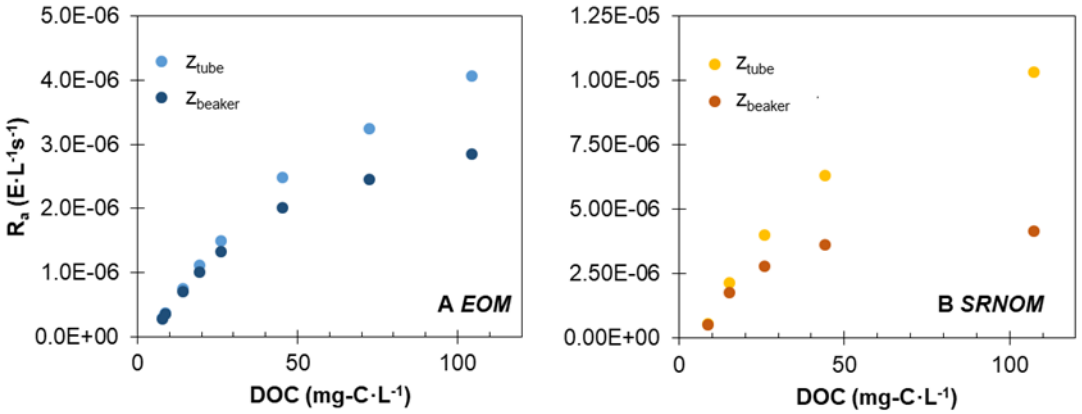

Figure S10. Rate of light absorption (R_a) in (A) EOM and (B) SRNOM solutions for pathlengths z_{beaker} = 3.0 cm ($^3DOM^*$ and $^1O_2$ quantification) and z_{tube} = 1.0 cm (HO• quantification).

Table S7. Additional EOM solution characterization including dissolved organic carbon (DOC_{TOTAL}), DOC contributed by EOM (DOC_{EOM} = DOC_{TOTAL} - DOC_{EDTA}, where DOC_{EDTA} = 7.6 mg-C·L^{-1}), absorbance at 254 nm ($A_{254,TOTAL}$), absorbance contributed by EOM ($A_{254,EOM}$ = $A_{254,TOTAL}$ – $A_{254,GROWTH\ MEDIUM}$, where $A_{254,GROWTH\ MEDIUM}$ = 0.165), specific UV absorbance at 254 nm in EOM ($SUVA_{254,EOM}$ = $A_{254,EOM}$/DOC_{EOM}), and the fluorescence index (FI). Values are the average of replicate measurements from January 2015 and July 2015 cultivations. Error represents the distance between minimum and maximum values from the average. FI was measured from July 2015 EOM solutions. EOM solutions were diluted to 90% (v_{sample}·v_{final}^{-1}) prior to use in irradiation experiments due to addition of molecular probes in deionized water. Thus, multiplying DOC and A_{254} values by a factor of 0.9 yields the conditions in irradiation experiments.

Day	DOC_{TOTAL} (mg-C·L^{-1})	DOC_{EOM} (mg-C·L^{-1})	$A_{254,TOTAL}$	$A_{254,EOM}$	$SUVA_{254,EOM}$ (L·mg-C^{-1}·m^{-1})	FI
0	8.78 ± 0.35	1.16	0.175 ± 0.005	0.010	1.08 ± 0.75	2.07
1	9.48 ± 0.89	1.86	0.186 ± 0.005	0.021	1.28 ± 0.37	---
2	15.7 ± 0.7	8.06	0.215 ± 0.004	0.050	0.63 ± 0.11	2.07
3	21.7 ± 0.1	14.0	0.249 ± 0.003	0.084	0.60 ± 0.03	---
4	29.1 ± 0.9	21.4	0.303 ± 0.001	0.138	0.64 ± 0.02	2.01
6	50.3 ± 1.9	42.6	0.456 ± 0.003	0.291	0.68 ± 0.02	---
8	80.6 ± 0.4	73.0	0.645 ± 0.009	0.480	0.66 ± 0.02	---
10	116 ± 2.6	108	0.928 ± 0.032	0.763	0.70 ± 0.01	1.84

Table S8. Additional SRNOM solution characterization including dissolved organic carbon (DOC_{TOTAL}), DOC contributed by SRNOM ($DOC_{SRNOM} = DOC_{TOTAL} - DOC_{EDTA}$, where $DOC_{EDTA} = 7.6$ mg-C·L^{-1}), absorbance at 254 nm ($A_{254,TOTAL}$), absorbance contributed by SRNOM ($A_{254,SRNOM} = A_{254,TOTAL} - A_{254,Fe+EDTA+NaHCO3}$, where $A_{254,Fe+EDTA+NaHCO3} = 0.139$), specific UV absorbance at 254 nm in SRNOM ($SUVA_{254,SRNOM} = A_{254,SRNOM}/DOC_{SRNOM}$), and the fluorescence index (FI). DOC and A_{254} values correspond to conditions in irradiation experiments.

DOC_{TOTAL} (mg-C·L^{-1})	$A_{254,TOTAL}$	DOC_{SRNOM} (mg-C·L^{-1})	$A_{254,SRNOM}$	$SUVA_{254,SRNOM}$ (L mg C^{-1} m^{-1})	FI
8.76	0.225	1.90	0.086	4.50	1.42
15.3	0.528	8.45	0.389	4.60	---
26.0	0.961	19.1	0.822	4.30	---
44.1	1.680	37.2	1.541	4.14	---
107	---	100	---	---	---

Table S9. Production of $^3DOM^*$, HO•, and $^1O_2$ in TAP growth medium and Fe-EDTA control experiments represented by $k_{obs,TMP}$, $R^{HO\bullet}$, and $[^1O_2]_{ss}$, respectively. Values are corrected for light screening. TAP medium error represents one standard deviation from triplicate measurements and Fe-EDTA error represents the distance between minimum and maximum values from the average.

Reactive Species Value	TAP Medium	Fe-EDTA
$k_{obs,TMP}$ (h^{-1})	0.031 ± 0.015	0.039 ± 0.001
$R^{HO\bullet}$ (pM·s^{-1})	18.3 ± 7.8	63.0 ± 8.6
$[^1O_2]_{ss}$ (fM)	6.36 ± 3.09	33.13 ± 1.20

Table S10. Additional characterization including pH, alkalinity, total carbonate ($C_{T,CO3}$) in the extracellular matrix, and biomass protein content. pH, alkalinity, and $C_{T,CO3}$ values are the average of replicate measurements from January 2015 and July 2015 cultivations. Error represents the distance between minimum and maximum values from the average. Protein was calculated using the nitrogen fraction and protein factor measured in July 2015 samples and the average volatile suspended solids (VSS) of replicate cultivations (January 2015 and July 2015). Error was combined from standard deviations of triplicate VSS measurements and the distance between minimum and maximum values from replicate nitrogen fraction measurements.

Day	pH	Alkalinity (mM)	$C_{T,CO3}$ (mM)	Protein (g·L^{-1})
0	8.57 ± 0.27	10.16 ± 1.36	10.13 ± 1.39	---
1	8.34 ± 0.04	8.76 ± 1.16	8.75 ± 1.17	0.19 ± 0.03
2	8.45 ± 0.04	4.43 ± 0.33	4.42 ± 0.34	0.51 ± 0.01
3	8.58 ± 0.09	4.35 ± 0.35	4.35 ± 0.35	0.54 ± 0.06
4	8.59 ± 0.02	4.30 ± 0.40	4.30 ± 0.40	0.55 ± 0.08
6	8.62 ± 0.02	4.30 ± 0.40	4.30 ± 0.40	0.52 ± 0.08
8	8.59 ± 0.00	4.40 ± 0.30	4.40 ± 0.30	0.47 ± 0.09
10	8.56 ± 0.03	4.40 ± 0.20	4.40 ± 0.20	0.54 ± 0.11

S4.2 Estimating MS2 Inactivation by Singlet Oxygen ($^1O_2$). Correlations between MS2 bacteriophage inactivation first-order rate constants ($k_{obs,MS2}$) and $[^1O_2]_{ss}$ (M) for several DOM isolates developed by Rosado-Lausell et al. were used to predict a $k_{obs,MS2}$ (h^{-1}) value.[11]

$$k_{obs,MS2} = 7.09 \times 10^{12}[^1O_2]_{ss} + 0.31 \quad (49)$$

When inputting a value of $[^1O_2]_{ss} = 10^{-13}$ M into the model (i.e., the highest order of magnitude of $[^1O_2]_{ss}$ found for EOM solutions in this study) we obtain $k_{obs,MS2} = 0.31$ h^{-1}. By definition, the $k_{obs,MS2}$ is the slope obtained from plotting ln (PFU/mL) versus time (h), where PFU is a plaque forming unit.[9,11,33] To estimate the required contact time for 2-log inactivation, we use Equation 50.

$$k_{obs,MS2} = \frac{ln(PFU/mL)}{time} \quad (50)$$

Rearranging, we obtain the following.

$$time = \frac{ln(PFU/mL)}{k_{obs,MS2}} \quad (51)$$

Converting 2-log inactivation (log (PFU/mL) = 2) to exponential form (ln (PFU/mL) = 4.605) and using this value in Equation 51 yields t = 5.6 h, or the time required for 2-log inactivation of MS2 at $[^1O_2]_{ss} = 10^{-13}$ M.

S4.3 Comparing Sensitized Reactive Species Photoproduction in EOM Solutions During and Post-Early Stationary Phase. $k_{obs,TMP}$, $R^{HO\bullet}$, and $[^1O_2]_{ss}$ were measured for the solution of EOM from the July 2015 replicate at day 10 (EOM_{dilute}) diluted from stationary phase DOC_{EOM} level (106 mg-C·L^{-1}; 95.2 mg-C·L^{-1} in irradiation experiments after 90% dilution, $v_{sample}{\cdot}v_{final}^{-1}$) to levels found in the early stationary phase (19.6 mg-C·L^{-1}; 17.6 mg-C·L^{-1} in irradiation experiments after 90% dilution, $v_{sample}{\cdot}v_{final}^{-1}$) to compare reactive species photoproduction at similar DOC_{EOM} (additional data are provided in Figure S11). The dilution was made using a solution containing $[Fe^{3+}]$ = 18 µM (the concentration in TAP growth medium, 20 µM diluted to 90%, $v_{sample}{\cdot}v_{final}^{-1}$), DOC_{EDTA} = 6.9 mg-C·L^{-1} (DOC originating from EDTA in the TAP growth medium, 7.6 mg-C·L^{-1} diluted to 90%, $v_{sample}{\cdot}v_{final}^{-1}$), $NaHCO_3$ = 4 mM, and was adjusted to pH ~ 8.0 to maintain a consistent background matrix comparable to EOM solutions in irradiation experiments. The DOC_{EOM} dilution factor was 5.4, but $k_{obs,TMP}$, $R^{HO\bullet}$, and $[^1O_2]_{ss}$ decreased by factors of 2.3, 1.4, and 4.7, respectively, suggesting that DOC_{EOM} in phase IV produced more reactive species than DOC_{EOM} in phase III.

Because of potential $^3DOM^*$ quenching phenomena, $k_{obs,TMP}$ was not expected to decrease proportionally with DOC.[10] Therefore, the discrepant decrease in $k_{obs,TMP}$ with dilution may not indicate greater reactive species production in EOM phase IV. The $R^{HO\bullet}$ was greater in EOM_{dilute} than the EOM solution in phase III as a result of two possible occurrences: (1) the EOM solution

in phase III produces less HO• than EOM solution in phase IV due to a lack of humic substance-like carbon in the former (Figure 2; main text), or (2) the EOM solution in phase IV is a significant HO• scavenger outcompeting benzene and the scavenging effect is less dramatic upon EOM dilution. Further investigation is needed to elucidate this mechanism. $[^1O_2]_{ss}$ decreased the most consistently with DOC_{EOM} dilution, however EOM_{dilute} produced 40.3% more $[^1O_2]_{ss}$ than the EOM solution in early stationary phase (Figure S11), indicating that the EOM solution in phase IV also produced greater $^1O_2$ levels. Lastly, though the EOM solution in phase IV produced greater $R^{HO\bullet}$ and $[^1O_2]_{ss}$ than the EOM solution in phase III at similar DOC_{EOM} concentrations, values were still not greater than those produced in the SRNOM solution at a comparable DOC_{SRNOM} concentration suggesting that SRNOM-enhanced photoreactivity will be greater than EOM-enhanced photoreactivity at any growth phase at an equivalent DOC concentration.

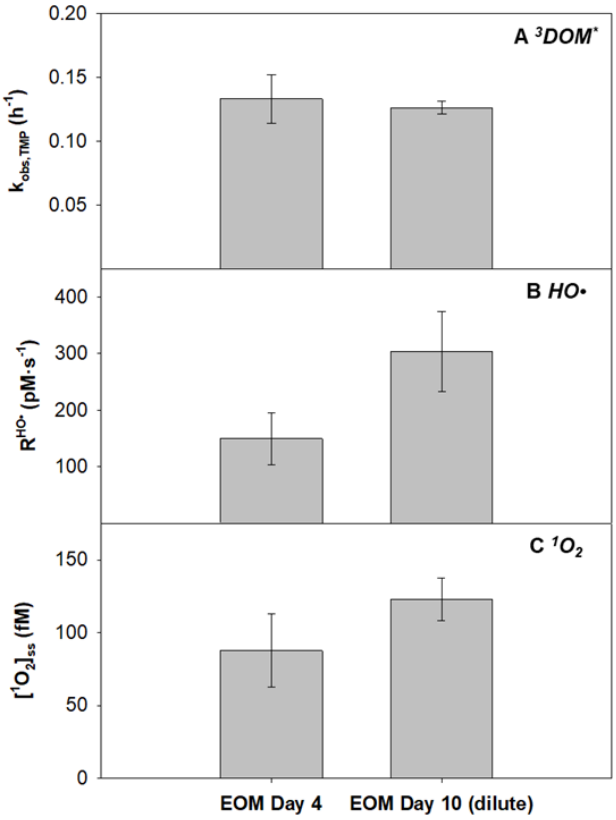

Figure S11. Production of $^3DOM^*$, HO•, and $^1O_2$ represented by (A) $k_{obs,TMP}$, (B) $R^{HO\bullet}$, and (C) $[^1O_2]_{ss}$, respectively, in a dilute sample of EOM collected at day 10 (EOM day 10 (dilute); right column) containing DOC_{EOM} = 17.6 mg-C·L^{-1} (19.6 mg-C·L^{-1} diluted to 90%, $v_{sample} \cdot v_{final}^{-1}$), $[Fe^{3+}]$ = 18 µM (20 µM diluted to 90%, $v_{sample} \cdot v_{final}^{-1}$), DOC_{EDTA} = 6.9 mg-C·L^{-1} (7.6 mg-C·L^{-1} diluted to 90%, $v_{sample} \cdot v_{final}^{-1}$), and $NaHCO_3$ = 4 mM at pH ~ 8. Error bars for EOM day 10 (dilute) represent one standard deviation from triplicate measurements using EOM solutions from the July 2015 cultivation. $k_{obs,TMP}$, $R^{HO\bullet}$, and $[^1O_2]_{ss}$ produced in the EOM solution at day 4 (EOM Day 4) containing DOC_{EOM} = 19.3 mg-C·L^{-1} (21.4 mg-C·L^{-1} diluted to 90%, $v_{sample} \cdot v_{final}^{-1}$) are shown for comparison (left column), with error bars that represent one standard deviation across biological replicates (January 2015 and July 2015) with triplicate measurements. Values were corrected for light screening.

References Cited in ESI

1 S. O. Lourenço, E. Barbarino, U. M. L. Marquez and E. Aidar, *J. Phycol.*, 1998, **34**, 798–811.
2 N. R. Boyle and J. A. Morgan, *BMC Syst. Biol.*, 2009, **3**, 4.
3 M. Grandbois, D. E. Latch and K. McNeill, *Environ. Sci. Technol.*, 2008, **42**, 9184–9190.
4 R. P. Schwarzenbach, P. M. Gschwend and D. M. Imboden, *Environmental Organic Chemistry*, John Wiley & Sons, Hoboken, NJ, 2003.
5 O. C. Romero, A. P. Straub, T. Kohn and T. H. Nguyen, *Environ. Sci. Technol.*, 2011, **45**, 10385–10393.
6 M. M. Dong and F. L. Rosario-Ortiz, *Environ. Sci. Technol.*, 2012, **46**, 3788–3794.
7 F. J. Beltran, G. Ovejero, J. F. Garcia-Araya and J. Rivas, *Ind. Eng. Chem. Res.*, 1995, **34**, 1607–1615.
8 X. Li, J. Ma, G. Liu, J. Fang, S. Yue, Y. Guan, L. Chen and X. Liu, *Environ. Sci. Technol.*, 2012, **46**, 7342–7349.
9 T. Kohn and K. L. Nelson, *Environ. Sci. Technol.*, 2007, **41**, 192–197.
10 X.-Z. Niu, C. Liu, L. Gutierrez and J.-P. Croué, *Water Res.*, 2014, **66**, 140–148.
11 S. L. Rosado-Lausell, H. Wang, L. Gutiérrez, O. C. Romero-Maraccini, X.-Z. Niu, K. Y. H. Gin, J.-P. Croué and T. H. Nguyen, *Water Res.*, 2013, **47**, 4869–4879.
12 C. S. Foote, J. S. Valentine, A. Greenberg and J. F. Liebman, *Active Oxygen in Chemistry*, Springer Netherlands, Dordrecht, Netherlands, 1995.
13 W. R. Haag and J. Hoigne, *Environ. Sci. Technol.*, 1986, **20**, 341–348.
14 W. R. Haag, J. Hoigne, E. Gassman and A. Braun, *Chemosphere*, 1984, **13**, 631–640.
15 E. Appiani, R. Ossola, D. E. Latch, P. R. Erickson and K. McNeill, *Environ. Sci. Process. Impacts*, 2017, **19**, 507–516.
16 S. Canonica, U. Jans, K. Stemmler and J. Hoigne, *Environ. Sci. Technol.*, 1995, **29**, 1822–1831.
17 S. Canonica and M. Freiburghaus, *Environ. Sci. Technol.*, 2001, **35**, 690–695.
18 M. S. Elovitz and U. von Gunten, *Ozone Sci. Eng.*, 1999, **21**, 239–260.
19 J. T. Jasper and D. L. Sedlak, *Environ. Sci. Technol.*, 2013, **47**, 10781–10790.
20 D. Vione, G. Falletti, V. Maurino, C. Minero, E. Pelizzetti, M. Malandrino, R. Ajassa, R.-I. Olariu and C. Arsene, *Environ. Sci. Technol.*, 2006, **40**, 3775–3781.
21 A. W. Vermilyea and B. M. Voelker, *Environ. Sci. Technol.*, 2009, **43**, 6927–6933.
22 J. J. Guerard, Y.-P. Chin, H. Mash and C. M. Hadad, *Environ. Sci. Technol.*, 2009, **43**, 8587–8592.
23 S. E. Page, W. A. Arnold and K. McNeill, *J. Environ. Monit.*, 2010, **12**, 1658–1665.
24 J. E. Donham, E. J. Rosenfeldt and K. R. Wigginton, *Environ. Sci. Process. Impacts*, 2014, **16**, 764–769.
25 G. McKay, J. L. Kleinman, K. M. Johnston, M. M. Dong, F. L. Rosario-Ortiz and S. P. Mezyk, *J. Soils Sediments*, 2014, **14**, 298–304.
26 G. McKay, M. M. Dong, J. L. Kleinman, S. P. Mezyk and F. L. Rosario-Ortiz, *Environ. Sci. Technol.*, 2011, **45**, 6932–6937.
27 J. V. Goldstone, M. J. Pullin, S. Bertilsson and B. M. Voelker, *Environ. Sci. Technol.*, 2002, **36**, 364–372.
28 G. V. Buxton, C. L. Greenstock, W. P. Helman and A. B. Ross, *J. Phys. Chem. Ref. Data*, 1988, **17**, 513–886.
29 L. M. Dorfman, I. A. Taub and R. E. Bühler, *J. Chem. Phys.*, 2004, **36**, 3051–3061.
30 K. K. Baduru, S. Trapp and J. G. Burken, *Environ. Sci. Technol.*, 2008, **42**, 1268–1275.
31 L. C. Bodhipaksha, C. M. Sharpless, Y.-P. Chin, M. Sander, W. K. Langston and A. A. MacKay, *Environ. Sci. Technol.*, 2015, **49**, 3453–3463.
32 R. M. Dalrymple, A. K. Carfagno and C. M. Sharpless, *Environ. Sci. Technol.*, 2010, **44**, 5824–5829.
33 R. J. Davies-Colley, A. M. Donnison, D. J. Speed, C. M. Ross and J. W. Nagels, *Water Res.*, 1999, **33**, 1220–1230.